Identification of structural controls in an active lava dome with high resolution DEMs: Volcán de Colima, Mexico

M. R. James[1] and N. Varley[2]

(1) Lancaster Environment Centre, Lancaster University, Lancaster, U.K. LA1 4YQ

(2) Facultad de Ciencias, Universidad de Colima, Bernal Díaz del Castillo #340, Colima, Mexico

Abstract

Monitoring the topography of active lava domes is critical for detecting changes that may trigger or influence collapse or explosive activity. Internal dome structure and conditions are more difficult to elucidate, but also play vital roles. Here, we describe the exposure (following an explosion) of significant scarps in the active dome at Volcán de Colima, Mexico, that are interpreted as evidence of brittle failure planes and a complex internal dome morphology. In the first use of automated 3D computer vision reconstruction techniques (structure-from-motion and multi-view stereo, SfM-MVS) on an active volcanic dome, we derive high resolution surface models from oblique and archive photographs taken with a consumer camera. The resulting 3D models were geo-referenced using features identified in a web-sourced orthoimage; no ground-based measurements were required. In December 2010, the dome (2.14×10^6 m^3) had a flat upper surface, reflecting an overall ductile emplacement regime. Between then and May 2011, a period of low explosivity was accompanied by a small volume loss (0.4×10^5 m^3) and arcuate steps appeared in the dome surface, suggesting the presence of localized planes of weakness. The complex array of summit scarps was exposed following a significant explosion in June 2011, and is interpreted to be the surface expression of fault planes in the dome. The 1-m resolution DEMs indicated that the region of greatest volume loss was not coincident with the assumed location of the conduit, and that heterogeneity within the dome may have been important during the June explosion.

1. Introduction.

Many growing lava domes present significant hazards due to their potential for explosive activity or collapse. A primary measurement required for forecasting such events is that of the dome topography, from which the volume of collapsible material can be constrained, and

effusion rate changes, that may signify a switch from effusive to explosive regimes, to be detected. However, internal parameters such as crust thickness, core-to-talus ratio and structural variability [e.g. *Fink et al*., 1990; *Buisson & Merle*, 2005; *Wadge et al.* 2008] are also of importance. Modern numerical models that include such complexities [*Hale et al*., 2009] have highlighted of the need for increasingly detailed field observations and surface data in an effort to improve our understanding of dome processes.

However, technical and practical limitations can make detailed topographic models of active volcanic flows and domes difficult to obtain. Traditional aerial photogrammetry [e.g. *Fink et al*., 1990; *Schilling et al.*, 2008] and aerial and ground-based laser scanning [*Jones*, 2006; *James et al.*, 2009; *Favalli et al.*, 2010] can provide high resolution data (e. g. measurement densities of order 1 m^{-2}, with decimetric errors), but are associated with significant costs and can be restricted by cloud and visibility. Ground-based radar can observe through cloud [*Wadge et al.*, 2005; *Macfarlane et al.*, 2012], but with spatial resolutions usually an order of magnitude lower than those from optical or laser techniques. Digital elevation models (DEMs) can also be derived from oblique photographs taken below the cloud base using consumer digital cameras. Such approaches based on photogrammetry (which require some pre-calibration of the camera and control points with known coordinates to be observable in the images) have been used for semi-automated reconstructions of volcanic edifices [*Cecchi*, 2003] and active lava flows [*James et al.*, 2007]. Similar techniques, but using manual surface point selection, have been used for dome volume estimation [*Herd et al.*, 2005; *Ryan et al.*, 2010; *Diefenbach et al.*, 2012]. However, manual selection is time consuming and thus not practical for delivering high resolution DEMs.

Here, we use a computer-vision based 3D surface reconstruction technique that has advantages over traditional photogrammetric approaches in that camera calibration and control point data are not required for initial model generation, and data processing is highly automated, typically delivering 10^6-10^7 surface point measurements within a few hours. In the absence of control data, initial models are at an undefined scale in an arbitrary coordinate system, so some control measurements are required for subsequent geo-referencing. Although the accuracies and precisions of the technique are less than those potentially delivered by precision photogrammetry, they do approach those achievable with a single stereo-pair [*James and Robson*, 2012].

We derive high resolution (e.g. average measurement densities of ~10 m^{-2}) surface models of the Volcán de Colima lava dome, spanning 2011(Figure 1a) in order to characterize surface changes and features that provide insight to internal dome structure. Archive images from 2007 (Figure 1b) were also processed, to visualize the location of the small early dome and to derive a pre-dome DEM.

2. Volcán de Colima

Volcán de Colima is a stratocone volcano located in western Mexico, approximately 30 km from the city of Colima. The most recent eruptive period at Colima has, so far, comprised four episodes characterized by dome growth (1998-9, 2001-3, 2004 and 2007-2011 [*Varley et al.*, 2010]). The first and third episodes were characterized by an effusion rate comparable to typical crater domes, whilst the second and most recent domes grew very slowly (~0.02 m^3 s^{-1} for 2007-2010 [Hutchinson *et al*. 2012]). By late 2009 during the most recent episode, the shallow summit crater had been mostly infilled and the growing dome began to overflow the crater to the west and, to a lesser extent, to the north and south. With a relatively flat upper surface, the

axisymmetric dome (Figure 1) indicates that overall emplacement morphology was controlled by ductile flow and the pressure in the conduit [*González-Mellado et al.*, 2011]. On 21 June 2011, a significant explosion heralded the cessation of dome growth and marked the end of the most recent eruptive episode. The volcano has been remarkably quiet since, with minimal degassing and seismicity registered.

3. Data and methods

The images used for DEM creation (Figure 1) were taken through an open window during four over-flights in a light aircraft (Table 1). Each image set was processed to produce a dense 3D point cloud surface model (Figure 1c) using computer vision 'structure-from-motion' and 'multi-view stereo' (SfM-MVS) algorithms. This technique was first applied to active volcanic systems by *James et al.* [2012] and further details and analyses of the accuracies involved are given by *James and Robson* [2012] and references therein. Appendix A describes the specific software used here.

To geo-reference the resulting 3D models, 5 features were identified in an orthorectified aerial image from Bing (available in ArcMap as a basemap layer), that were also observable in the image sets. With a pixel resolution of order a meter, the orthoimage provided suitable planimetric constraints (although we have no knowledge of its orthorectification quality), but no vertical control. Consequently, the relative *z*-coordinates of the control points were defined by rotating the model so that the approximately flat upper surface of the 12 December 2010 dome was horizontal. The updated *xyz* control point coordinates were then used to geo-reference the other surveys.

The resulting 3D errors on the control features had RMS values <2 m (Table 1), which provides an indication of the overall precision of the horizontal registration with respect to the

orthoimage, and of the vertical precision between different surveys. However, SfM-MVS has been shown to deliver measurement precisions of order 1/1000 of the viewing distance [*James and Robson*, 2012] so, for most of the surveys the models are expected to be internally consistent to precisions closer to ~1 m. Thus, prior to model comparisons, an iterative closest point technique (as commonly used for laser scanner data) was used to optimize the relative registration of models by minimizing offsets with respect to the December 2010 survey, over areas of known static topography (the SSW to NE portion of the flanks and crater rim, Figure 2a). DEMs (Figure 2a) were then produced by gridding the point clouds over a 1-meter-resolution grid and comparisons of the static regions give RMS differences of 0.62 – 1.22 m (Table 1, see also Figure 2b and c). If an estimated worst-case error of a 1 m systematic vertical offset between surfaces is assumed, corresponding volume errors for the dome would be 2.8 – 3.2% for 2010 and 2011, and 4.4% for 2007. To produce a pre-eruptive surface for comparisons, a copy of the 2007 survey was made in which the data representing the small dome (Figure 1b) were replaced by a flat surface to approximate the crater floor (Figure 2d).

4. Results and discussion

All DEMs show the dome centered on a location offset from the center of the existing crater by ~30 m to the NW (Figure 3b). This matches the growth of previous domes and suggests a complex architecture to the upper conduit, with effusion occurring from different offset vents [*Lavallée et al.*, 2012]. The calculated surfaces and dome volumes show volumetric loss during 2010 (Table 1), despite substantial growth (~10 m thickness) of talus to the north in the latter half of the year (Figure 2). The small decrease in dome volume and height between December 2010 and May 2011 was accompanied by the appearance of gentle arcuate and concentric topographic structures on the dome surface (Figure 1a middle panel, Figure 2b). The nature of

these features suggests that they represent regions of localized deformation in the dome, and their formation is thus probably related to the process of volume loss during this period. However, the means of volume loss is undetermined. The lack of vigorous vulcanian activity during this period discounts explosive excavation, leaving continued overflow of the dome to the west, dome compaction, or some magma withdrawal into the conduit as potential alternatives. Magma withdrawal or compaction (only a 2% loss of vesicularity in the dome would suffice) may be difficult to reconcile with the pressurization that must have been occurring prior to the June explosion. If continued overflow to the west was responsible, the distribution of volume loss (Figure 2b) indicates that the bulk of the dome was able to slump westwards. This also offers a small degree of unloading as a potential trigger for the June explosion.

The June event left a complex dome surface with multiple high angled scarps suggesting the presence of fault planes (i.e. brittle deformation features in the dome carapace) or highly localized shear (Figure 3). Scarps towards the eastern and southern extremities are parallel to and ~10 m from the edge of dome, indicating detachment of central regions from a likely cooler exterior. Their curved nature is reminiscent of the active ring fractures at Santiaguito dome [*Bluth and Rose,* 2004] through which eruptions emanate. However, closer to the center of the dome, structures with a general NNE-SSW trend are present. Previous observations on the inactive 1991 dome showed evidence of N-S striking faults (J. C. Gavilanes and A. Cortés, pers. comm.), and a similar direction was noted for a graben-like structure that formed within the early stages of both the 2001-3 and 2007-11 domes. Although this trend agrees with the alignment of regional tectonics [*Norini et al.,* 2010], within the dome, it may also be affected by the main (westerly) overflow direction.

The DEMs also show that the deepest part of the post-explosion depression (at A', Figure 2d) is offset from the center of the dome and thus, by implication, also offset from the active conduit. This could suggest that heterogeneities in the dome, potentially due to pre-existing structures or to variability in magma rheology during dome construction, were significant in the June explosion. Thus, despite the overall ductile emplacement morphology indicated by the relatively flat upper surface of the dome, the effects of internal variabilities should not be neglected when considering explosion and collapse events. The modeling of block and ash flows at Colima has shown the potential impact of dome collapses [*Sulpizio et al.*, 2010]; however, structural details of the upper edifice are not yet considered in such models and could magnify flow volumes and run out distances.

5. Conclusions

High resolution DEMs of the volcanic dome at Volcán de Colima have been acquired using a new photo-reconstruction technique, SfM-MVS. The DEMs quantify a small subsidence of the dome surface prior to a significant vulcanian explosion in June 2011, and allow the mapping of linear and arcuate failure planes evident within the dome following the explosion, that may provide zones of weakness in further events. Asymmetry of the post-explosion dome topography suggests that internal dome heterogeneity was important during the explosion and thus further efforts should be made to incorporate internal variability into dome hazard assessments.

Appendix A: SfM-MVS software

Two different software implementations were used for SfM-MVS processing. Images from 2007, 2010 and May 2011 were processed with the 'Bundler Photogrammetry Package' (http://blog.neonascent.net/archives/bundler-photogrammetry-package/), as described by *James and Robson* [2012]. To carry out a reconstruction, image files were copied into a project folder

along with two run-scripts, which were then executed. The resulting 3D models were geo-referenced using sfm_georef (http://www.lancs.ac.uk/staff/jamesm/software/sfm_georef.htm [*James and Robson*, 2012]), that calculates and applies a transformation (a scaling, rotation and translation) based on three or more control points identified in the image set.

The images for December 2011 were more challenging to process because of blurring and large variations in image scale (zoom); Bundler only assimilated 42 images into the model and limited the reconstruction to the East portion of the dome and crater. Consequently, the web site Photosynth.net was used to carry out the initial SfM processing step. Photosynth can often assimilate more images into a model than Bundler, but usually at the expense of reconstruction accuracy. 'PhotoSynthToolkit9' (http://www.visual-experiments.com/2012/04/) was then used to export the Photosynth results and run the subsequent MVS step. Geo-referencing was carried out with sfm_georef. Although coverage was better than from Bundler, some sub-sections of the model were noticeably misaligned. Nevertheless, overlaps with neighboring regions allowed refinement (by iterative closest-point adjustment) to create one consistent surface.

Acknowledgemements

We thank Clement Thorey and Mike Black who took the photographs in 2011. We are grateful to S. Anderson and an anonymous reviewer for their constructive comments on the paper.

References

Bluth, G. J. S., and W. I. Rose (2004) Observations of eruptive activity at Santiaguito volcano, Guatemala, *J. Volc. Geotherm. Res.*, 136, 297-302.

Buisson, C., and O. Merle (2005), Influence of crust thickness on dome destabilization, *Geol. Soc. Am. Sp. Pap.*, 396, 181-188.

Cecchi, E. (2003), Reconstruction 3D pour la volcanologie: apports d'une méthode multi-vues par photogrammétrie numérique, PhD thesis, University of Clermont-Ferrand, Clermont-Ferrand.

Diefenbach, A., K. F. Bull, R. L. Wessels, and R. G. McGimsey (2012), Photogrammetric monitoring of lava dome growth during the 2009 eruption of Redoubt Volcano, *J. Volcanol. Geotherm. Res.*, doi: 10.1016/j.jvolgeores.2011.12.009.

Favalli, M., A. Fornaciai, F. Mazzarini, A. Harris, M. Neri, B. Behncke, M. T. Pareschi, S. Tarquini, and E. Boschi (2010), Evolution of an active lava flow field using a multitemporal LIDAR acquisition, *J. Geophys. Res.*, 115, B11203, doi: 10.1029/2010jb007463.

Fink, J. H., M. C. Malin and S. W. Anderson (1990) Intrusive and extrusive growth of the Mount St-Helens lava dome, *Nature*, 348, 435-437.

González-Mellado, A. O., S. De La Cruz-Reyna, and C. Navarro-Ochoa (2011), Applications of a simplified equation of state for the density of silicate hydrous magmas: The Volcán de Colima (Mexico) buoyancy-driven dome growth process Similarities and differences with the Popocatépetl volcano domes, *J. Volcanol. Geotherm. Res.*, 205, 17-29, doi: 10.1016/j.jvolgeores.2011.03.009.

Hale, A. J., E. S. Calder, G. Wadge, S. C. Loughlin, and G. A. Ryan (2009), Modelling the lava dome extruded at Soufrière Hills Volcano, Montserrat, August 2005–May 2006, J. Volcanol. Geotherm. Res., 187, 53-68, doi: 10.1016/j.volgeores.2009.08.023.

Herd, R. A., M. Edmonds, and V. A. Bass (2005), Catastrophic lava dome failure at Soufriere Hills Volcano, Montserrat, 12-13 July 2003, *J. Volcanol. Geotherm. Res.*, 148, 234-252, doi: 10.1016/j.jvolgeores.2005.05.003.

Hutchinson, W., N. Varley, D. M. Pyle, and T. A. Mather (2012), Airborne thermal remote sensing of the Volcán de Colima (Mexico) lava dome from 2007 to 2010, *Geological Society Spec. Pub., in press.*

James, M. R., L. J. Applegarth, and H. Pinkerton (2012), Lava channel roofing, overflows, breaches and switching: insights from the 2008-9 eruption of Mt. Etna, *Bull. Volc.*, 74, 107-117, doi: 10.1007/s00445-011-0513-9.

James, M. R., H. Pinkerton, and S. Robson (2007), Image-based measurement of flux variation in distal regions of active lava flows, *Geochem. Geophys. Geosyst.*, 8, Q03006, doi: 10.1029/2006GC001448.

James, M. R., H. Pinkerton, and L. J. Applegarth (2009), Detecting the development of active lava flow fields with a very-long-range terrestrial laser scanner and thermal imagery, *Geophys. Res. Lett.*, 36, L22305, doi: 10.1029/2009gl040701.

James, M. R., and S. Robson (2012), Straightforward reconstruction of 3D surfaces and topography with a camera: Accuracy and geoscience application, *J. Geophys. Res.*, 117, F03017, doi: 10.1029/2011JF002289.

Jones, L. D. (2006), Monitoring landslides in hazardous terrain using terrestrial LiDAR: an example from Montserrat, *Quart. J. Eng. Geology Hydrol.*, 39, 371-373.

Lavallée, Y., N. R. Varley, M. A. Alatorre-Ibargüengoitia, K.-U. Hess, U. Kueppers, S. Mueller, D. Richard, B. Scheu, O. Spieler, and D. B. Dingwell (2012), Magmatic architecture of dome-building eruptions at Volcán de Colima, Mexico, *Bull. Volcanol.*, 74, 249-260, doi: 10.1007/s00445-011-0518-4.

Macfarlane, D. G., H. M. Odbert, D. A. Robertson, M. R. James, H. Pinkerton, and G. Wadge (2012), Topographic and thermal mapping of volcanic terrain using the AVTIS ground based 94GHz dual-mode radar/radiometric imager, *IEEE Trans. Geosci. Remote Sensing*, in press, doi: 10.1109/TGRS.2012.2202667.

Norini, G., L. Capra, G. Groppelli, F. Agliardi, A. Pola, and A. Cortes (2010), Structural architecture of the Colima Volcanic Complex, *J. Geophys. Res.*, 115, B12209, doi: 10.1029/2010JB007649.

Ryan, G. A., S. C. Loughlin, M. R. James, L. D. Jones, E. S. Calder, T. Christopher, M. H. Strutt, and G. Wadge (2010), Growth of the lava dome and extrusion rates at Soufriere Hills Volcano, Montserrat, West Indies: 2005-2008, *Geophys. Res. Lett.*, 37, L00E08, doi: 10.1029/2009gl041477.

Schilling, S. P., R. A. Thompson, J. A. Messerich, and E. Y. Iwatsubo (2008), Use of digital aerophotogrammetry to determine rates of lava dome growth, Mount St. Helens, Washington, 2004–2005, in *A Volcano Rekindled: The Renewed Eruption of Mount St. Helens, 2004-2006*, vol. 1750, edited by D. R. Sherrod, et al., pp. 145-167, U.S. Geological Survey Professional Paper.

Sulpizio, R., L. Capra, D. Sarocchi, R. Saucedo, J. C. Gavilanes-Ruiz, and N. R. Varley (2010), Predicting the block-and-ash flow inundation areas at Volcán de Colima (Colima, Mexico)

based on the present day (February 2010) status, *J. Volcanol. Geotherm. Res.*, 193, 49-66, doi: 10.1016/j.jvolgeores.2010.03.007.

Varley, N., R. Arámbula-Mendoza, G. Reyes-Dávila, R. Sanderson, and J. Stevenson (2010), Generation of Vulcanian activity and long-period seismicity at Volcán de Colima, Mexico, *J. Volcanol. Geotherm. Res.*, 198, 45-56, doi: 10.1016/j.jvolgeores.2010.08.009.

Wadge, G., D. G. Macfarlane, D. A. Robertson, A. J. Hale, H. Pinkerton, R. V. Burrell, G. E. Norton, and M. R. James (2005), AVTIS: a novel millimetre-wave ground based instrument for volcano remote sensing, *J. Volcanol. Geotherm. Res.*, 146, 307-318, doi: 310.1016/j.jvolgeores.2005.1003.1003.

Wadge, G., D. G. Macfarlane, H. M. Odbert, M. R. James, J. K. Hole, G. Ryan, V. Bass, S. De Angelis, H. Pinkerton, D. A. Robertson, and S. C. Loughlin (2008), Lava dome growth and mass wasting measured by a time series of ground-based radar and seismicity observations, *J. Geophys. Res.*, 113, B08210, doi: 10.1029/2007jb005466.

Figures

Figure 1 (a) Example images used from each 2010 and 2011 survey. The dashed white cross sections (A – A' – A") indicates a reference section taken through all resulting models (see Figure 2). Arrows in the first panel show the location of features used for geo-referencing. (b) Example image used from 2007, in the early stages of dome growth. (c) An oblique view of the 3D point cloud model derived for 15 May 2011, looking to the NNE (white areas represent no data).

Figure 2. (a) A shaded relief map of the 26 December 2010 DEM; coordinates are UTM. The region to the east enclosed by the dashed line indicates the area of static crater flanks topography that was used for relative registration of the surfaces. Maps of vertical change since 26 Dec. 2010 are given for 27 May 2011 (b), and 26 Dec. 2011(c); note the different color scales. White areas indicate elevation change of less than ±0.2 m, the significant apparent elevation changes on the inner east wall of the crater result from low data coverage due to shadowing. The position of the original crater rim is given by the thick dashed grey line. (c) Cross sections showing the 2011 subsidence of the dome surface. The dashed portion of the 2007 section indicates the assumed pre-dome surface used in the total volume calculations (Table 1).

Figure 3. (a) Excerpt of an image from 26 December 2011, looking northeast over the complex structures on the dome surface. (b) A shaded relief model of the associated DEM, overlain with a map of the major structural features on the dome. Dashed black lines show the outline of more subtle gradient changes or minor explosion craters. The red-shaded area indicates the location of the dome near the beginning of the eruption on 15 November 2007, with the thick dashed grey line giving the position of the crater rim.

Table 1. Survey details and calculated dome volumes

Date	Number of images (used successfully)	Average viewing distance, m	Average point density[c], m^{-2}	RMS error on control, m, (number of points)	RMS difference over crater rim[d], m	Dome volume, $\times 10^6$ m^3 (DRE[g])
15 Nov. 2007	58 (45)[a]	505	4.1	1.45 (5)	1.22[f]	0.15 (0.12[h])
26 Dec. 2010	28 (28)[b]	1160	11.1	1.66 (5)	--	2.14 (1.66-1.25)
27 May 2011	114 (114)[b]	910	45.1	1.48 (5)	0.39	2.10 (1.64-1.23)
26 Dec. 2011	192 (190)[b]	2420	18.9	1.30 (3[e])	0.62	1.91 (1.47-1.10)

[a] Konica Minolta Dimage Z5 (5 M pixels) camera; [b] Nikon D90 (12.9 M pixels) camera and 18-105 mm lens; [c] Calculated within a circular region of radius of 120 m from dome center; [d] Area analyzed shown in Figure 2a; [e] Two control points overrun by dome activity; [f] Due to lack of coverage in 2007 images, no area north of 2157170 is included; [g] Dense rock equivalent (DRE) volumes calculated using a lava porosity of 16% [*Lavallée et al.*, 2012] and assuming talus is ~63% clasts [e.g. *Wadge et al*., 2008]. The range reflects the difference between representing the region of core dome material as a cylinder or inverted cone below the upper dome surface; [h] Assumes negligible talus component.

Figure 1 James & Varley

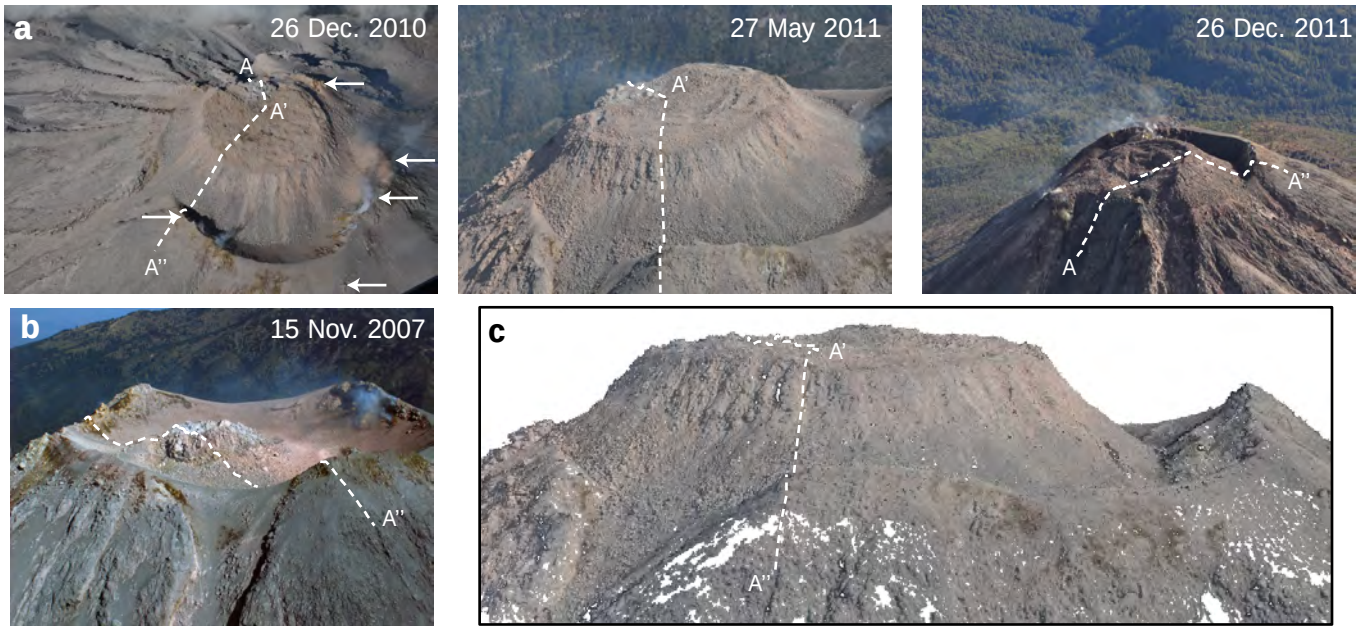

Figure 2 James & Varley

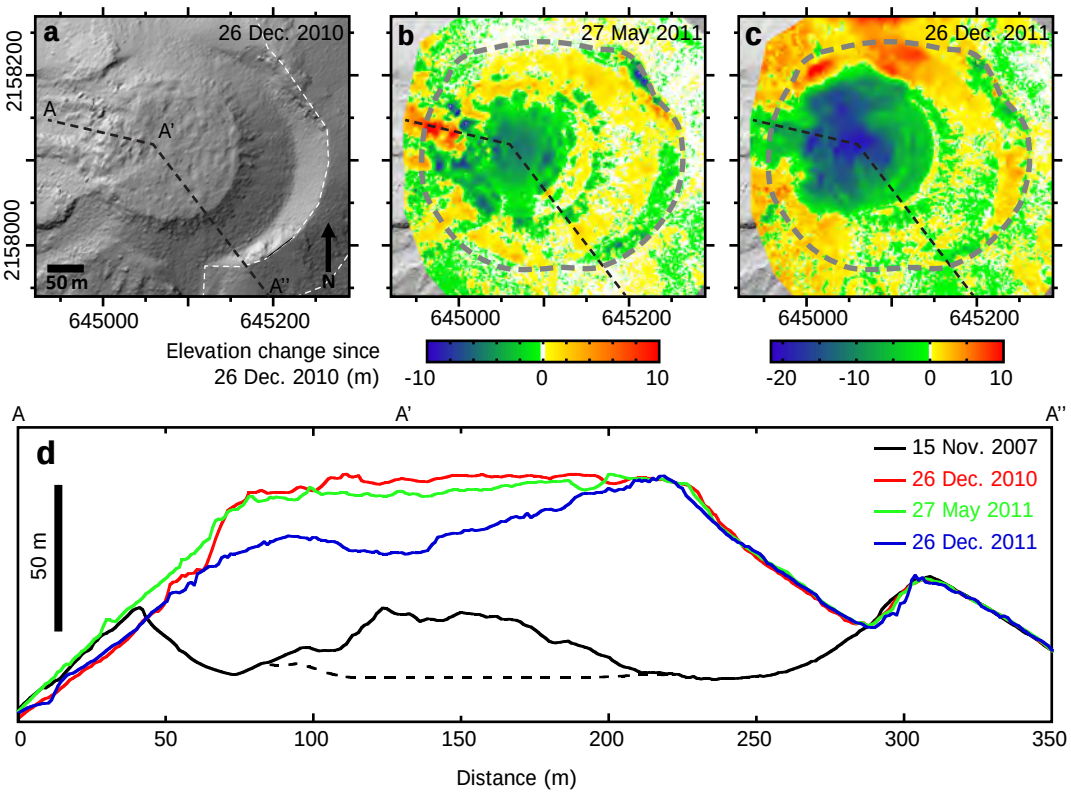

Figure 3 James & Varley